CHEMISTRY
A European Journal

A Journal of
ChemPubSoc Europe

Accepted Article

Title: Solution conformations explain the chameleonic behaviour of macrocyclic drugs

Authors: Emma Danelius, Vasanthanathan Poongavanam, Stefan Peintner, Lianne Wieske, Mate Erdelyi, and Jan Kihlberg

To be cited as: *Chem. Eur. J.* 10.1002/chem.201905599

Link to VoR: http://dx.doi.org/10.1002/chem.201905599

Supported by
ACES

WILEY-VCH

10.1002/chem.201905599

WILEY-VCH

Solution Conformations Explain the Chameleonic Behavior of Macrocyclic Drugs

Emma Danelius,[†][a] Vasanthanathan Poongavanam,[†][a] Stefan Peintner,[a] Lianne H.E. Wieske,[a] Máté Erdélyi,*[a] and Jan Kihlberg*[a]

[a] Dr. E. Danelius,[†] Dr. V. Poongavanam,[†] S. Peintner, L. Wieske, Prof. M. Erdélyi,* Prof. J Kihlberg*
Department of Chemistry-BMC
Uppsala University
SE-75123, Uppsala, Sweden
E-mail: mate.erdelyi@kemi.uu.se and jan.kihlberg@kemi.uu.se

[†] These authors contributed equally to this work

Supporting information for this article is given via a link at the end of the document.

Abstract: It has been hypothesized that drugs in the chemical space beyond the rule of 5 (bRo5) must behave as molecular chameleons to combine otherwise conflicting properties, including aqueous solubility, cell permeability and target binding. Evidence for this has, however, been limited to the cyclic peptide cyclosporin A. Herein we show that the non-peptidic and macrocyclic drugs roxithromycin, telithromycin and spiramycin behave as molecular chameleons, with rifampicin showing a less pronounced behavior. In particular roxithromycin, telithromycin and spiramycin display a marked, yet limited flexibility and populate significantly less polar and more compact conformational ensembles in an apolar than in a polar environment. In addition to balancing of membrane permeability and aqueous solubility, this flexibility also allows binding to targets that vary in structure between species. The drugs' passive cell permeability correlates to their 3D polar surface area and corroborate two theoretical models for permeability, developed for cyclic peptides. We conclude that molecular chameleonicity should be incorporated in the design of orally administered drugs in the bRo5 space.

Introduction

The design of cell permeable and orally absorbed drugs has traditionally focused on the chemical space described by the Lipinski´s rule of 5 (Ro5).[1] However, at least half of all targets involved in human diseases have been considered unsuitable for modulation with Ro5 compliant small molecule drugs.[2] Targets with flat and featureless binding sites, including protein-protein interactions, are especially challenging.[3] Biologics are successfully used to modulate targets having such binding-sites, often with exceptional specificity and potency. However, they lack cell permeability and consequently cannot reach intracellular targets, nor can they be administered orally.

To bridge the gap between small molecules and biologics, compounds in the beyond rule of 5 (bRo5) space, such as peptides, peptidomimetics and macrocycles, are currently attracting major interest.[4-8] By analysis of a comprehensive set of >200 orally administered drugs and clinical candidates residing in bRo5 space we have shown that bRo5-ligands provide improved opportunities for the modulation of difficult-to-drug targets.[4, 9] Macrocycles stand out by their ability to modulate targets that have large, flat or groove-shaped binding sites.[9-10] Furthermore, the chemical space in which cell permeable and orally absorbed drugs are found has recently been shown to extend far beyond the Ro5 space.[4, 6-7] Thus, bRo5 compounds, and in particular macrocycles, can exhibit a combination of the advantageous properties of biologics and small molecule drugs. However, a general understanding and proper description of their features is still lacking.

Compounds in the bRo5 space have been hypothesized to undergo conformational changes that dynamically shield or expose polar functionalities in response to changes in the surrounding environment.[11-15] Such compounds have been termed 'molecular chameleons' and it has been suggested that their flexibility allows them to display properties, including potent binding to targets, high cell permeability and aqueous solubility, that otherwise would be mutually exclusive in bRo5 space.[13, 15] Interestingly, all approved oral drugs in the bRo5 space possess a certain degree of flexibility; supporting the notion that bRo5 drugs are able to adjust to the environment.[15] In addition, the analysis of crystal structures for a set of bRo5 drugs revealed a correlation between their passive cell permeability and their minimum solvent accessible 3D polar surface area, corroborating the hypothesis that drugs in this space behave as molecular chameleons.[15] However, with the exception of the macrocyclic peptide cyclosporine A,[11, 16] the conformational space of bRo5 drugs in solutions mimicking the cell membrane and the plasma/cytosol, and the relationship between conformations and properties, has not been studied experimentally for this class of compounds. This hinders both the qualitative understanding and the development of predictive models for property-based design in bRo5 chemical space.

Herein, we address this scientific gap by determining the solution conformational ensembles for a carefully selected set of orally available, non-peptidic macrocyclic drugs by an NMR spectroscopic technique proven to be successful for flexible compounds.[17-26] In-depth analysis of the ensembles obtained in both aqueous and apolar solutions provides broader experimental evidence that drugs in the bRo5 space behave as molecular chameleons. In addition, our studies suggest that conformational flexibility allows binding to targets that vary in structure between species and demonstrate that molecular chameleonicity correlates to passive cell permeability.

Results and Discussion

We have studied four cell permeable and structurally diverse macrocyclic drugs from the erythronolide, leucomycin and rifamycin classes of antibacterial agents (Figure 1). These macrocycles have one to three side-chains of varying flexibility and rings encompassing 15 to 25 atoms. Solutions in water, with the pH adjusted to approximately 7.0, and in chloroform were used in the NMR studies to mimic the plasma/cytosol and the cell membrane, respectively. Chloroform is often used in this

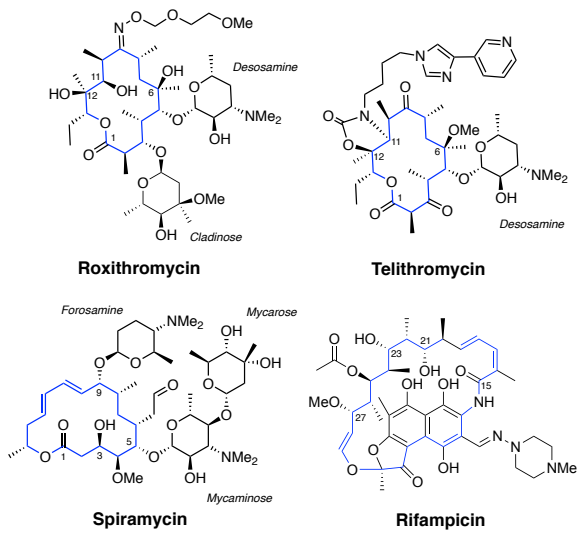

Figure 1. Structures of the four macrocyclic drugs for which conformational ensembles have been determined in $CDCl_3$ and D_2O. The macrocyclic core of each drug is highlighted in blue and the names of the attached saccharides are in italics.

respect as it has a dielectric constant (ε=4.8) close to that determined for a lipid bilayer (ε=3.0).[27] Roxithromycin, telithromycin and spiramycin contain tertiary amino groups and are protonated in water at this pH, while rifampicin is zwitterionic (cf. pK_a values in Table 4).[28] In chloroform the first three are in their neutral from, while rifampicin is non-ionic.[28]

The conformations of the four selected macrocycles have been studied by NMR spectroscopy in the 1970s to early 1990s. However, the treatment of time averaged chemical shifts (δs), coupling constants (*J*s), temperature coefficients ($\Delta\delta/\Delta T_{OH}$s), relaxation ($T_1$) data and nuclear Overhauser effects (NOEs) with the rudimentary techniques available at that time did not allow the description of solution ensembles as mixtures of rapidly interconverting conformations. Instead an approximate picture consisting of a single population averaged conformation was provided. In addition, the dependence of the conformational ensembles on the polarity of the environment was not systematically assessed. In these studies the solution conformation of roxithromycin in chloroform was found to be similar to that in the crystalline state, with the oxime chain being oriented towards the macrocyclic ring, and with some flexibility at the C2-C8 region.[29-31] Signs for conformational alteration were observed upon comparison of the NMR data obtained in chloroform to that in methanol and solution ensembles were proposed, but with limited certainty.[32] The conformation of telithromycin in aqueous solution has been analysed based on δs, *J*s, T_1 data and NOEs in combination with restrained MD calculations, providing helpful insights into the flexibility and geometry of the macrocycle, yet without being able to describe the composition of the solution ensemble.[33] The NMR assignment of spiramycin has been published, but its conformational ensembles have not been described.[34] Analysis of δs and *J*s for rifampicin suggested one preferred conformation in D_2O and at least two conformers in $CDCl_3$.[35] These conformations were formed by rotations of the amide bond and the C28-C29 double bond and were concluded to resemble the one in the crystalline state.

The above studies provided information on the overall, time-averaged geometry of these macrocycles; however, they were unable to describe the composition of the solution ensembles. To achieve this, we deconvoluted the time-averaged NMR data into individual solution conformations using the NAMFIS algorithm.[36] Conformational analysis by NAMFIS requires experimentally determined proton-proton distances obtained from NOE build-up measurements, and dihedral angles calculated from vicinal scalar couplings as input; this data was therefore generated for the four selected macrocycles (Supporting Information, Sections 1 and 2). NAMFIS has previously been successfully used to determine the solution conformations of Ro5-[17-18] and bRo5-compounds, including both peptides[19-22, 25-26] and macrocycles.[23-24]

NAMFIS also requires a theoretical conformational ensemble as input, which provides comprehensive coverage of the conformational space available for the compound being studied. We recently reported that conformational sampling of the charged form of drugs in bRo5 space, including roxithromycin and telithromycin, failed to identify crystal structures of the drugs investigated.[37] In addition, our initial attempts to determine the solution ensembles of roxithromycin succeeded when a theoretical conformational ensemble for the neutral form was used, but failed for an ensemble of the charged form. Based on these observations, and on several reports on the successful use of the theoretical ensembles of the neutral form of complex and charged compounds,[21, 25-26, 36] we generated theoretical ensembles for the neutral and non-ionic form of the four macrocycles studied herein. Unrestrained Monte Carlo conformational searches with different force fields and both water and chloroform solvent models produced comprehensive ensembles within an energy window of 42 kJ/mol (Supporting Information, Section 3). Crystal structures available from the PDB and CSD were added to ensure the best possible coverage of the theoretically available conformational space (Supporting Information, Section 4). Solution ensembles were then determined for the four macrocycles using the NAMFIS algorithm by varying the probability of each conformer in the theoretical input ensembles to find the best fit of the probability weighted back-calculated distances and dihedral angles to the experimental population-averaged values which had been derived from solution NMR data.

Since the conformations of highly flexible moieties are difficult to sample exhaustively by conformational search algorithms,[38] we initially included data only for the macrocyclic cores into the first step of the NAMFIS analyses. After having established the macrocycle core conformation, experimentally determined distances for side chains were also added. The limited ability of theoretical methods to describe the conformational space of the side chains, along with NOEs originating from difficult to assign diastereotopic protons, makes it most challenging to describe the side chain orientations with high accuracy. In spite of this the overall conformations, including the side chain orientations, could be validated for the four compounds by the addition of random noise to the experimental data, by the random removal of individual restraints, and by comparison of the experimentally observed and back-calculated distances.

The aqueous and chloroform solution ensembles for the four macrocycles are described in detail in the Supporting Information (Sections 5 and 6). We recently provided an initial description of the solution ensemble of roxithromycin in chloroform and water.[37] We have now improved this analysis by inclusion of crystal structures in the NAMFIS analysis and by determination of temperature coefficients for hydroxy groups, which provided a much improved description of the chloroform ensemble.

Roxithromycin

We identified six conformations for roxithromycin in aqueous solution. They span a diverse conformational space as determined by their pairwise RMSD values (Figure 2A, Supporting Information, Figure S5 and Table S23). The macrocycle cores of five of the conformations adopt structurally diverse geometries, with the cores of conformations 2 and 6

belonging to the same cluster (Figure 2C, Supporting Information, Table S23). In chloroform only one conformation was found (Figures. 2B and 2D), that has previously been observed in the crystalline state of roxithromycin (CSD: KAHWAT[39]). This conformation is also present in the aqueous ensemble (6%).

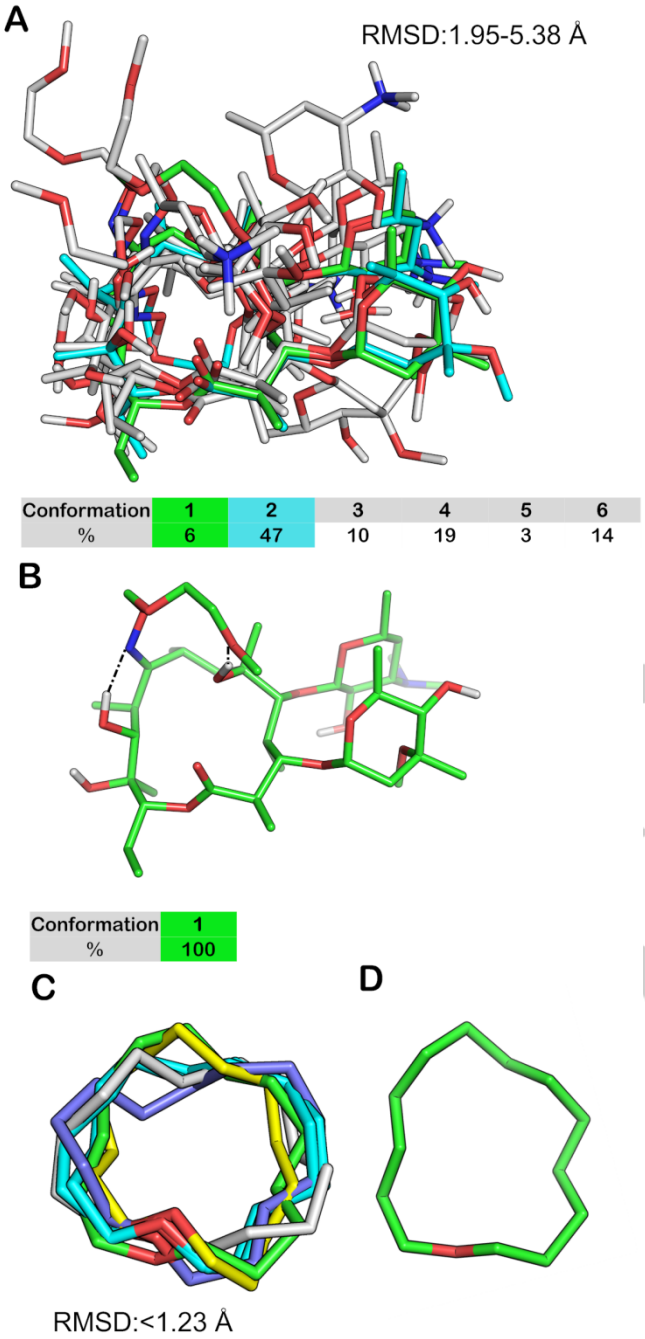

Figure 2. (**A**) and (**B**) Solution conformational ensembles of roxithromycin and their population (in %) in D_2O and $CDCl_3$, respectively. Roxithromycin is shown in protonated form in panel A and in neutral from in panel B. (**C**) and (**D**) Conformations adopted by the macrocycle core of roxithromycin in D_2O and $CDCl_3$, respectively. The most populated conformation in D_2O (no. 2) is in cyan in panels A and C. The single conformation found in $CDCl_3$ (no. 1), which is also part of the D_2O ensemble, is in green in all panels. The core of conformation 6 belongs to the same cluster as no. 2 and is also in cyan in panel C. In panel C the cores of conformations 3, 4 and 5 are in grey, yellow and purple, respectively. Intramolecular hydrogen bonds to the oxime side chain are indicated with dotted lines in panel B. Figures in panels A-D were obtained by overlaying the atoms of the macrocycle core, and nonpolar hydrogen atoms were omitted for clarity. RMSD values were calculated for heavy atoms.

A large number of NOEs indicate major differences in the orientation of the flexible side chains of roxithromycin in the two solvents (Figure 2A and 2B). Whereas the available data did not allow a detailed quantification of the molar fractions of different side chain orientations, it provides a robust qualitative description (Supporting Information, Section 8). Hence, in aqueous solution the oxime side chain adopts diverse orientations. It is solvent exposed in 75% of the solution conformations (nos. 2, 3, 5 and 6), and folded over the macrocycle core or the attached desosamine and cladinose moieties in two conformers (no. 1 and 4). As judged by the torsional angles for its glycosidic bonds, the desosamine moiety is fairly rigid in relation to the macrocycle core (Table 1, Supporting Information, Table S29). In contrast, the cladinose moiety displays greater flexibility around its Ψ_H angle. Originating from the flexibility of the macrocycle and that of the two monosaccharides, the saccharides are stacked in two conformations (no. 1 and 2) that represent approximately half of the ensemble and protrude away from the macrocycle core in the other half of the ensemble.

In the single conformation found in chloroform (no. 1), the desosamine and cladinose moieties are stacked against each other and the oxime side chain is folded over the macrocycle core (Figure 2B). This results in formation of intramolecular hydrogen bonds (IMHBs) to two of the three hydroxy groups of the core (6-OH and 11-OH). The temperature coefficients for the five hydroxy groups of roxithromycin reveals that both 6-OH (-6.2 ppb K^{-1}) and 11-OH (-5.3 ppb K^{-1}) form IMHBs of weak to intermediate strength in chloroform, most likely to the flexible oxime side chain (Supporting Information, Tables S27 and S28). Our analysis suggests that the three remaining hydroxy groups (12-, 2'- and 4''-OH) form strong IMHBs (-1.8 -> -2.4 ppb K^{-1}), likely through formation of pseudo-five membered rings to adjacent oxygen atoms.

Table 1. Torsional angles for the glycosidic bonds between the cladinose and desosamine moieties and the macrocycle core of roxithromycin and telithromycin.[a]

Drug	Solvent	Cladinose		Desosamine	
		Φ_H[b]	Ψ_H[c]	Φ_H[b]	Ψ_H[c]
Roxithromycin	D_2O	45 (6)	20 (4), -25 (1), -164 (1)	46 (6)	10 (4), -14 (2)
	$CDCl_3$	45 (1)	35 (1)	49 (1)	10 (1)
Telithromycin	D_2O			52 (5) 166 (2)	15 (5) 29 (2)
	$CDCl_3$			53 (7)	12 (6), -4 (1)

[a] Torsional angles are averages of the angles for conformations that have similar staggered orientations about Φ_H and Ψ_H. Data for all conformations is given in the Supporting information (Supporting Information, Tables S29 and S30). The number of conformations that have contributed to the averages is given in parenthesis. [b] Φ_H = H_1-C_1-O_1-C_x. [c]. Ψ_H = H_x-C_x-O_1-C_1

The experimentally determined solution ensembles thus reveal that roxithromycin is significantly more flexible and adopts structurally diverse conformations in water, whereas it exists as a single conformation in chloroform. When transitioning from water into chloroform, the oxime side chain reorients from being predominantly solvent exposed to a closed conformation with two intramolecular hydrogen bonds to the macrocycle core. Similarly, the desosamine and cladinose moieties orient to be stacked against each other. These conformational changes synergistically reduce the polarity of roxithromycin, which is expected to increase its cell permeability.

Telithromycin

The solution ensembles of telithromycin consist of seven conformations each in aqueous and in chloroform solutions (Figure 3A and 3B, Supporting Information, Figures S7 and S8). The *E. coli* ribosome bound conformation of telithromycin (no. 7 - PDB: 4V7S[40]) is present to 5% in water, while the *T. thermophilus*' and *S. aureus'* ribosome bound conformations constitute the dominant conformers of the chloroform ensemble [no. 13 – PDB: 4V7Z[41] (52%) and no. 14 – PDB: 4WF9[42] (16%)]. In contrast to roxithromycin, the aqueous and chloroform ensembles have comparable overall structural diversity, when judged by RMSD values (Figure 3A and 3B, Supporting Information, Table S24). Two clusters with different macrocycle core geometries, each comprising approximately 50% of the ensemble, were identified among the seven aqueous conformations (Figure 3C, Supporting Information, Table S24). The RMSD values of the core atoms of the conformations in the aqueous ensemble range up to 0.73 Å, revealing that the core of telithromycin is less flexible than that of roxithromycin in their aqueous ensembles. In chloroform, the cores of all but two conformations (no. 11 and 12), which comprise only 6% of the ensemble, belong to the same cluster (Figure 3D). Just as for roxithromycin, the core of telithromycin is thus less flexible in chloroform than in water.

Quantifiable NOEs of the side chains of telithromycin allowed the detailed quantitative description of their orientations in the two ensembles. In chloroform, the aromatic side chain of telithromycin is oriented over the macrocycle in three of the minor conformations in chloroform (nos. 10, 12 and 14), while stacking with the macrocyclic ring in the major conformation (no. 13). These four conformations, which represent 77% of the ensemble, may be stabilized by van der Waals interactions between the aromatic ring and the non-polar moieties of telithromycin, such as the methyl group at O-6 in the core and the C-6 methyl of the desosamine moiety. In water only one conformation (no. 1, 5%) has the aromatic ring oriented towards the macrocycle. The desosamine moiety orients away from the macrocyclic core in all aqueous and chloroform conformations. The Φ_H and Ψ_H torsional angles suggest that this sugar is fairly rigid in relation to the macrocycle core in both solvents (Table 1, Supporting Information Table S30).

Overall, the macrocyclic core of telithromycin is less flexible in chloroform than in water, and in chloroform its aromatic side chain is folded over the macrocycle core to a significantly larger extent than in water. Even if somewhat less pronounced than for roxithromycin, telithromycin thus also adopts a more open and flexible ensemble in a polar as compared to a non-polar environment.

Spiramycin

Spiramycin exists in three conformations in water and four in chloroform (Figure 4A and 4B, Supporting Information, Figures S9 and S10). The major conformation in the aqueous ensemble (no. 3, 68%) is identical to its structure in the complex with a macrolide phosphotransferase of *E. coli* (PDB: 5IGZ[43]), while the conformer reported for its complex with the 50S ribosomal subunit of *H. marismortui* (no. 7, PDB: 1KD1[44]) is the minor conformer in chloroform (11%). The aqueous and chloroform ensembles show comparable overall structural diversity, with RMSD values between the conformations in each ensemble ranging up to 4.6 Å (Figure 4A and 4B, Supporting Information Table S25). In water and chloroform the macrocycle core clusters into two and three conformational families, respectively (Figure 4C and 4D). The RMSD of the core heavy atoms of these ensembles range up to 0.7 Å in both environments (Supporting Information Table S25).

The inclusion or exclusion of the side chain NOEs during the analysis provided identical solution ensembles for each of

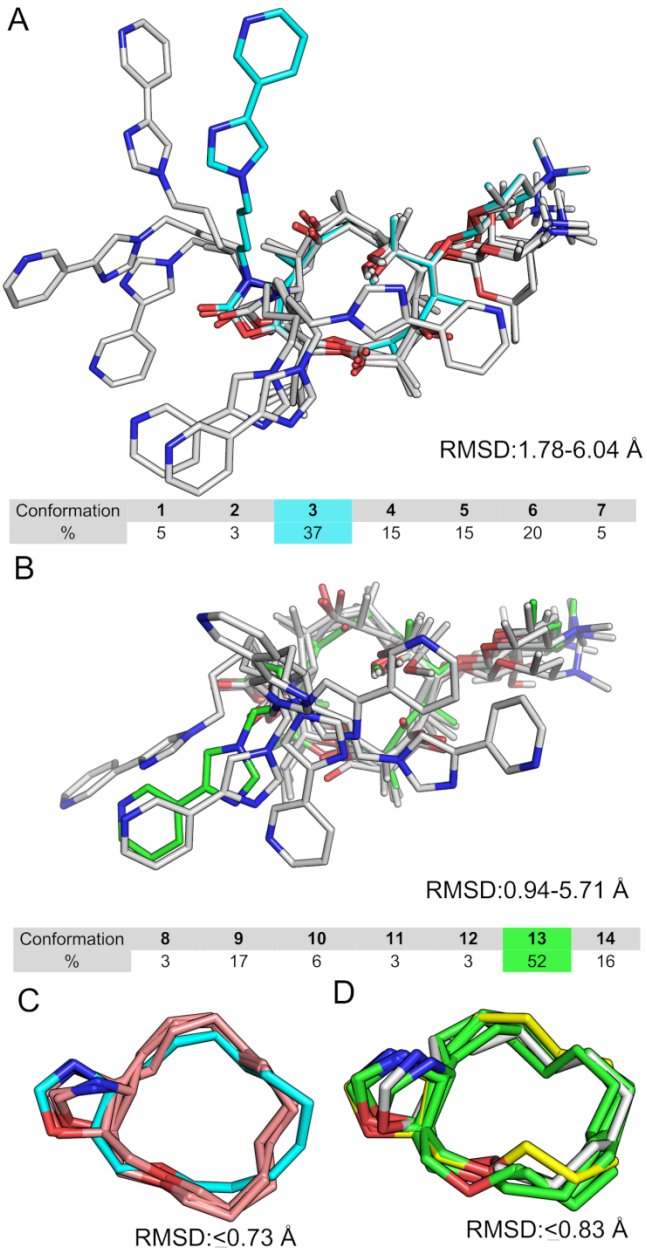

Figure 3. (**A**) and (**B**) Solution conformational ensembles of telithromycin and their population (in %) in D_2O and $CDCl_3$, respectively. Teliithromycin is shown in protonated form in panel A and in neutral from in panel B. (**C**) and (**D**) Conformations adopted by the macrocycle core of telithromycin in D_2O and $CDCl_3$, respectively. The most populated conformation in D_2O (no. 3) is in cyan in panels A and C, while the most populated conformation in $CDCl_3$ is in green in panels B and D. In panels C and D the cores of the conformations are coloured by cluster, i.e. cyan (3 and 6) and maroon (1, 2, 4, 5 and 7) for D_2O (panel C), and green (8, 9, 10, 13 and 14), yellow (11) and grey (12) for $CDCl_3$ (panel D). Figures in panels A-D were obtained by overlaying the atoms of the macrocycle core, and nonpolar hydrogen atoms were omitted for clarity. RMSD values were calculated for heavy atoms.

chloroform and water, respectively. Despite the unavoidable challenges in the description of the orientation of the flexible side chains, the ensemble obtained in chloroform was very robust. The side chain orientations in water were determined based on seven NOEs and are of good quality. Thus, the core conformation is well sampled by the conformational search and is accurately described by the NMR data in both solutions. The orientations of the more flexible saccharide side chains are also well characterized in chloroform, but somewhat uncertain in water.

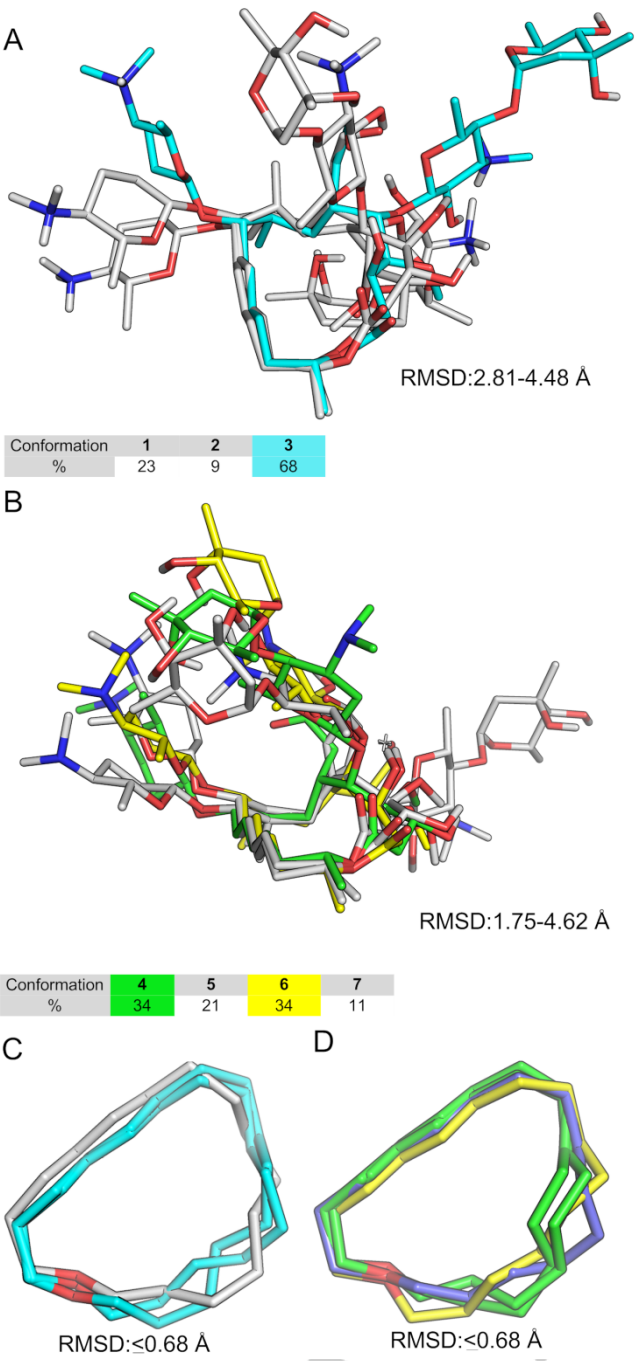

Figure 4. (**A**) and (**B**) Solution conformational ensembles of spiramycin and their population (in %) in D_2O and $CDCl_3$, respectively. Spiramycin is shown in diprotonated form in panel A and in neutral from in panel B. (**C**) and (**D**) Conformations adopted by the macrocycle core of spiramycin in D_2O and $CDCl_3$, respectively. The most populated conformation in D_2O (no. 3) is in cyan in panel A. In panel C the core of conformation 2, which belongs to the same cluster as no. 3, is also in cyan. The most populated conformations in $CDCl_3$ are in green and yellow in panels B and D. In panel D the core of conformation no. 5 which belongs to the same cluster as no. 4 is also in green, while conformation 7 is in purple. Figures in panels A-D were obtained by overlaying the atoms of the macrocycle core. Nonpolar hydrogen atoms were omitted for clarity. RMSD values were calculated for heavy atoms.

Major differences between the ensembles in water and chloroform were found for the orientations of the saccharide side chains (Table 2, Supporting Information Table S31) and the extent to which they form IMHBs with the macrocycle core. In water, the saccharides point away from the macrocycle in 77% of the ensemble (conformations 2 and 3), whereas they are oriented over the macrocycle and stacked against each other in

Table 2. Torsional angles for the glycosidic bonds of the three monosaccharides in spiramycin [a]

Sacharide	Solvent	Φ_H[b]	Ψ_H[c]
Forosamine	D_2O	42 (3)	25 (1), -51 (2)
	$CDCl_3$	48 (3)	33 (1), -40 (2)
		-44 (1)	27 (1)
Mycaminose	D_2O	55 (3)	33 (2), 161 (1)
	$CDCl_3$	47 (2)	32 (1), -39 (1)
		169 (2)	-13 (2)
Mycarose	D_2O	40 (3)	30 (3)
	$CDCl_3$	24 (4)	32 (2), 164 (1) -54 (1)

[a] Torsional angles are averages of the angles for conformations that have similar staggered orientations for Φ_H and Ψ_H. The number of conformations that have contributed to the averages is given in parenthesis. Data for all conformations is given in the Supporting information (Table S31). [b] $\Phi_H = H_1\text{-}C_1\text{-}O_1\text{-}C_x$. [c] $\Psi_H = H_x\text{-}C_x\text{-}O_1\text{-}C_1$

89% of the chloroform ensemble (conformations 4-6). These differences are also reflected by formation of IMHBs between the macrocycle and the mycaminose moiety in the two major conformations in chloroform that represent 68% of the ensemble. Conformation 4 has an IMHB between OH-2 of mycaminose and the carbonyl group of the macrocycle lactone, while conformation 6 has an IMHB between the anomeric oxygen of mycaminose and OH-3 in the macrocycle. In water, only the minor conformation (no. 2, 9%) displays an IMHB analogous to that of conformer 6 in chloroform.

Just as the two erythronolides, spiramycin undergoes a conformational change from a more open, solvent exposed aqueous ensemble, in which the two saccharides point away from each other and from the macrocycle core, to a more closed and solvent shielded ensemble in chloroform. In the latter ensemble the saccharides are stacked, with IMHBs between the mycaminose moiety and the macrocycle core in the dominant conformers. As already, mentioned such conformational changes are expected to reduce polarity thereby improving membrane permeability.

Rifampicin

The aqueous solution ensemble of rifampicin consists of five conformers, and the chloroform ensemble of three (Figure 5A and 5B, Supporting Information, Figures S11 and S12). Four crystal structures were identified in the aqueous ensemble, which overall represent 89% of the ensemble. Hence, the CSD structures LOPZEX[45] and OWELOS[46] are identical to the solution conformers 2 and 3, whereas rifampicin's conformations when bound to RNA polymerase as reported in the structures 1YNN[47] (PDB) and 5HV1[48] (PDB) correspond to conformations 4 and 5, respectively. In chloroform solution, the crystal structure of rifampicin bound to the D13 scaffold protein from poxviruses (PDB: 6BED[49]) constitutes a minor conformation, representing 11% of the ensemble. Rifampicin has an overall lower flexibility as compared to the other three macrocycles studied herein, which is explained by its lack of large flexible side chains. The RMSD of the heavy atoms of its solution conformers ranges up to 2.9 Å (Figure 5A and 5B, Supporting Information Table S26). The macrocycle core of rifampicin populates three clusters of conformations in each solvent, characterized by RMSD values of 1-1.5 Å (Figure 5C and 5D, Supporting Information Table S26). This reveals the flexibility of the core to be comparable to that of roxithromycin in water, but higher than that of the cores of telithromycin and spiramycin in aqueous solution.

In chloroform, the aliphatic hydroxy groups OH-21 and OH-23 are solvent shielded by the nearby aromatic moiety in two conformations (no. 6 and 7), whereas in water they become

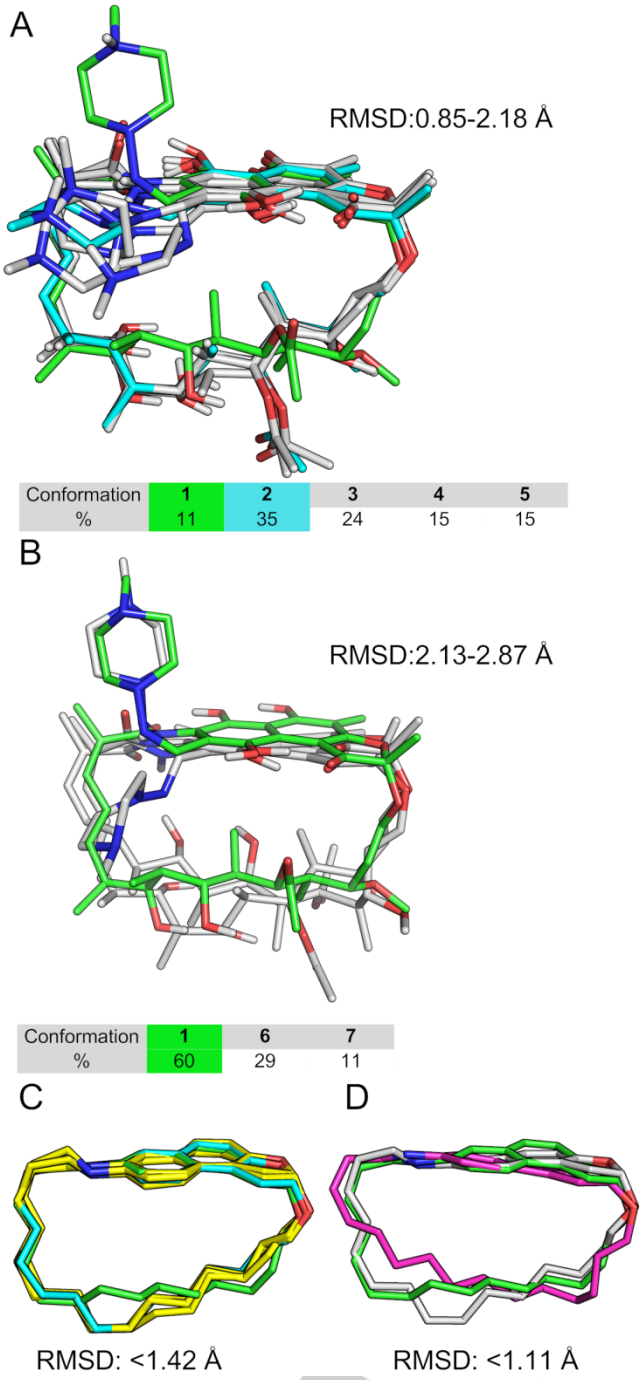

Figure 5. (**A**) and (**B**) Solution conformational ensembles of rifampicin and their population (in %) in D_2O and $CDCl_3$, respectively. Rifampicin is shown in its zwitterionic form in panel A and in non-ionic from in panel B. (**C**) and (**D**) Conformations adopted by the macrocycle core of rifampicin in D_2O and $CDCl_3$, respectively. The most populated conformation in D_2O (no. 2) is in cyan in panels A and C. The most populated conformation in $CDCl_3$ (no. 1), which is also populated in D_2O, is in green in all panels. The cores of conformations 3, 4 and 5 belong to one cluster and are in yellow in panel C. The cores conformations 6 and 7 are in grey and pink, respectively, in panel D. Figures in panels A-D were obtained by overlaying the atoms of the macrocycle core, and nonpolar hydrogen atoms were omitted for clarity. RMSD values were calculated for heavy atoms.

solvent exposed upon a conformational change of the macrocyclic core. The orientation of the piperazine side chain is not well described by the NMR data. However, five of the seven conformations populated by rifampicin are identical to crystal structures and the piperazine side chain orientations in the crystals were considered to be valid also in solution. As both chair and boat forms have been reported for the piperazine in crystal structures of rifampicin (chair in LOPZEX and OWELOS, boat in 3BED, 2HW2),[47-49] quantum mechanical calculations were performed for the two remaining conformations (1 and 6), both of which are populated in chloroform. Geometry optimization using DFT-B3LYP established both conformations to be more stable when the piperazine adopted a boat conformation (Supporting Information, Section 10), which also agrees with one of the best resolved crystal structures of rifampicin (2HW2, 1.45 Å).[50] Overall, the piperazine side chain resides in the plane of the aromatic moiety in all but the minor conformation (no.1) in water, but has a perpendicular orientation in the two major conformations in chloroform.

Rifampicin has a lower overall flexibility than the three other macrocycles, but it still adjusts its conformation in response to the polarity of the environment. The most notable changes are the adjustment of the aliphatic part of the macrocyclic core, altering the solvent exposure of its two hydroxy groups, and the reorientation of the piperazine side chain in relation to the aromatic moiety.

Comparison to target bound structures

Several studies of pharmacologically active compounds have found that the target bound bioactive conformation, is represented in the solution ensemble of the compound.[20, 24, 51-54] For roxithromycin, the only reported target bound crystal structure (PDB: 1JZZ,[55] *D. radiodurans*) was not found in the solution ensembles. However, the conformation of the macrocycle core in the target bound conformation is similar to the single conformation in chloroform, which is also populated to 6% in water (RMSD = 0.56 Å, conf. 1). In contrast, target bound structures are found in the solution ensembles of telithromycin, spiramycin and rifampicin (Table 3). Five ribosome bound crystal structures from different bacteria have been reported for telithromycin. One of them constitutes a minor conformation in water (4V7S[40]), another is the major conformation found in the chloroform ensemble (4V7Z[41]) while a third corresponds to a minor conformation in chloroform (4WF9[42]). The two target bound crystal structures available for spiramycin correspond to the major conformation in water (5IGZ[43]) and the minor one in chloroform (1KD1[44]). For rifampicin,[17] target bound crystal structures from six different organisms are available. They belong to four different bioactive conformations, three from crystal structures with different bacterial RNA polymerases and one with the D13 scaffold protein from vaccinia virus. Two of the three polymerase bound structures are found in the aqueous ensemble (1YNN,[47] 5HV1[48]), while the structure of rifampicin bound to vaccinia virus constitutes one of the minor conformations in chloroform (6BED[49]).

Table 3. Target bound structures in the solution ensembles of telithromycin, spiramycin and rifampicin[a]

	D_2O	$CDCl_3$
Telithromycin	**7** (5%): *E. coli* (4V7S)	**13** (52%): *T. thermophilus* (4V7Z)
		14 (16%): *S. aureus* (4WF9)
Spiramycin	**3** (68%): *E. coli* (5IGZ)	**7** (11%): *H. marismortui* (1KD1)
Rifampicin	**4** (15%): *T. aquaticus* (1YNN)	**7** (11%): V. virus (6BED)
	5 (15%): *E. coli* (5HV1)	

[a] For each drug the number of the conformation in the ensemble, its population in %, the organism from which the target originates and its PDB ID is given.

Telithromycin, spiramycin and rifampicin bind to targets from different organisms by adopting significantly different geometries (Figure 6). The resolution of these structures vary from 1.45 to

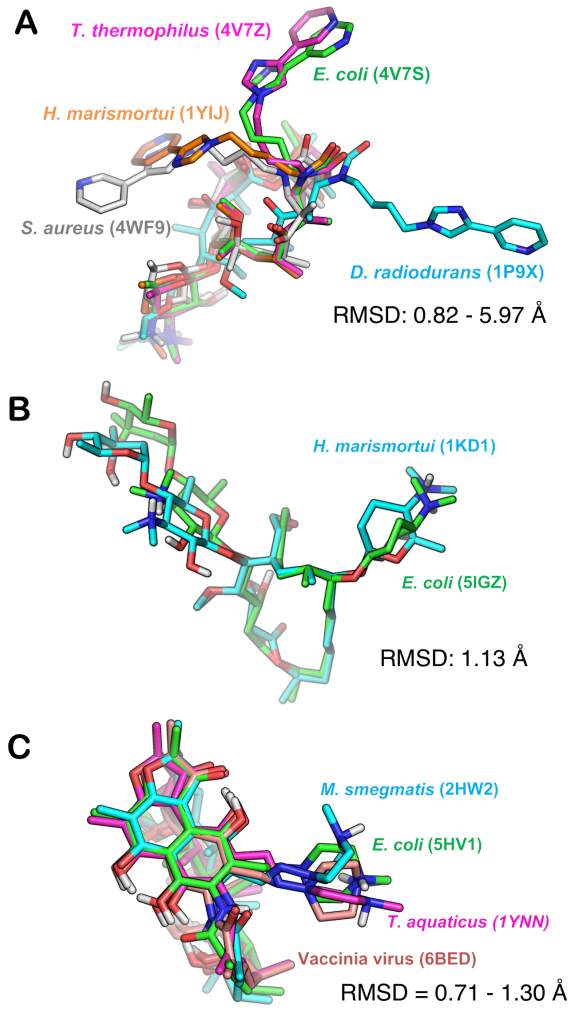

Figure 6. Overlays of reported target bound structures of (**A**) telithromycin, (**B**) spiramycin and (**C**) rifampicin, which display different bioactive conformations for each of the drugs. The name of the organism from which the target originates and the PDB ID of the crystal structures are given using the same colour as the corresponding structure in each overlay. The range of pairwise RMSD values between the heavy atoms of different conformations is also given. Figures were obtained by overlaying the atoms of the macrocycle core, and nonpolar hydrogen atoms were omitted for clarity.

3.4 Å. Electron density maps obtained at the lower resolution end of this range are often not sufficiently detailed to allow unambiguous identification of the conformation of the bound ligand, prompting us to inspect the final electron density maps (Supporting Information, Section 11). However, also for the low resolution crystal structures the observed map features support the modelled ligand orientation and the conformations of the ring substituents.

Telithromycin constitutes the most striking example as it adapts to ribosomes from different organisms in conformations that show major differences (Figure 6A, RMSD ≤6 Å). This is mainly due to the flexibility of the aromatic side chain, but also a result of conformational variation in the macrocycle core (RMSD ≤1.11 Å). The desosamine moiety and the core of telithromycin bind similarly to the different ribosomes, while the position of the aromatic side chain is determined by the polarity, shape and steric interactions in the binding site (Supporting Information, Figure S19). In the three elongated conformations of telithromycin (PDB ID: 4V7Z, 4V7S and 1P9X), which have a high solvent accessible 3D polar surface area (SA 3D PSA), the aromatic side chain is located in a polar pocket of the ribosome. For ribosomes where this pocket is less polar and smaller telithromycin instead adopts folded and less polar conformations (PDB ID: 1YIJ and 4WF9).

The target bound structures of spiramycin and rifampicin display smaller variations between conformers (Figures 6B and 6C). Each bioactive conformer of these two drugs share similar macrocycle core geometries (RMSD ≤0.58 Å), but differ in side chain orientation. Spiramycin is bound both by the bacterial ribosome and by the macrolide phosphotransferase that confers resistance to antibiotics. In both complexes the forosamine moiety and its amino group are solvent exposed, while the disaccharide is located in a polar pocket of the targets (Supporting Information, Figure S20) Rifampicin binds not only to different bacterial RNA polymerases, but also to the D13 protein from vaccinia virus. The polar piperazine side chain is solvent exposed in all structures (Supporting Information, Figure S21). The two structures having the highest resolution (PDB ID: 2HW2[50] and 6BED[49]), in which rifampicin shows a large structural variation (RMSD 1.29 Å), reveal that rifampicin is bound in conformations stabilized by multiple intramolecular hydrogen bonds and coordinated water. This allows rifampicin to bind to the predominantly nonpolar, but otherwise unrelated binding sites of RNA polymerase and the D13 protein from vaccinia virus. In summary, this analysis suggests that the flexibility of the three macrocycles allows them to bind to different targets, the binding sites of which display large differences in properties and structure. The conformational flexibility of molecular chameleons may thus provide potent binding to targets that vary in structure between species (e.g. telithromycin), and could even allow them to display polypharmacology (cf. rifampicin).

Descriptor based analysis of solution ensembles

The molecular radius of gyration (R_{gyr}),[56] describing the size of a compound, and its three-dimensional polar surface area (3D PSA)[15, 56] are descriptors that are useful to characterize molecular chameleons.[13, 15, 37] Both descriptors have a strong correlation to cell permeability, and the PSA also influences solubility.[15, 56] Knowledge of the conformational ensemble of a compound, including the orientations of the attached side chains, in an apolar environment is therefore of major importance for prediction of cell permeability. In analogy, the ensemble populated in water is expected to reflect the aqueous solubility.

As discussed above the conformations of the macrocyclic cores in the ensembles of all four drugs were determined with high reliability using NAMFIS analysis, both for chloroform and water solutions (cf. above). In addition, the conformations of the side chains were characterized with very high (telithromycin), high (spiramycin) or adequate (roxithromycin) reliability from the NMR data. For rifampicin the orientation of the piperazine side chain originated from crystal structures, and quantum chemical calculations. The in-depth knowledge of the overall ensembles of all four macrocycle drugs provides a strong foundation for descriptor calculations and correlations to cell permeability.

The radius of gyration R_{gyr} of a compound is calculated as the root-mean-square distance between its atoms and center of mass for each conformation adopted.[57] Consequently, conformational ensembles characterized by large differences in size between individual conformations display wide ranges of their R_{gyr} values. In agreement with this expectation, the structurally diverse ensembles of telithromycin and spiramycin had large R_{gyr} ranges (0.7-2.0 Å) both in water and chloroform (Figure 7A, Supporting Information Table S37).

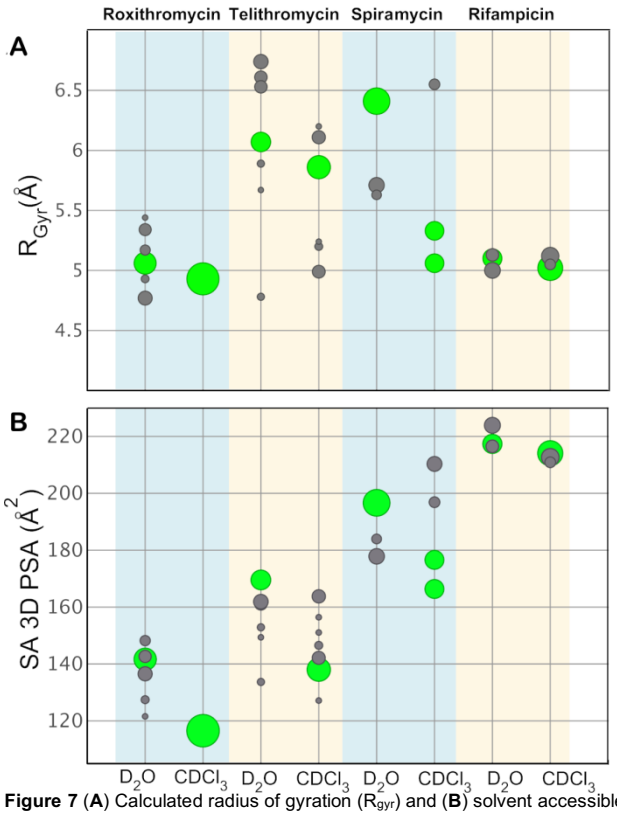

Figure 7 (**A**) Calculated radius of gyration (R_{gyr}) and (**B**) solvent accessible 3D polar surface area (SA 3D PSA) for the conformational ensembles of roxithromycin, telithromycin, spiramycin and rifampicin in D_2O and $CDCl_3$. The size of each circle is representative of the population (in %) of each conformation, and the circle corresponding to the major conformation of each ensemble is indicated in green. The SA 3D PSA was calculated for the protonated forms of roxithromycin, telithromycin and spiramycin in D_2O and for the neutral form in $CDCl_3$. For rifampicin the zwitterionic form was used in D_2O and the non-ionic form in $CDCl_3$.

Roxithromycin also showed a significant variation in R_{gyr} (appr. 0.7 Å) between the conformations populated in water, but adopts only one conformation in chloroform. Rifampicin, in contrast, has smaller R_{gyr} ranges (appr. 0.15 Å) in both solutions, reflecting a rigid macrocycle core and that it only carries one small side chain. It is notable that the major conformation of all four macrocyclic drugs has a lower R_{gyr} value in chloroform than in water, illustrating that all compounds adopt more compact conformations in an apolar environment. Spiramycin is the most striking example as its two saccharide side chains point away from each other in water, but are stacked in chloroform, while the rigid rifampicin shows only a minor difference between the environments. In addition, the R_{gyr} of all four drugs is below 7 Å, the proposed upper cutoff for cell permeability.[56]

The topological polar surface area (TPSA) is a descriptor of the polarity of compounds calculated from their 2D fragments, which provides a satisfactory descriptor of the polarity of compounds that comply with the Ro5.[58] For larger compounds in the bRo5 space, their solvent-accessible 3D polar surface area (SA 3D PSA) has been found to be a better descriptor of compound polarity.[15] The SA 3D PSA of the ensembles of the four macrocyclic drugs investigated herein showed a major increase from roxithromycin to rifampicin, and also a significant variation (≤45 Å^2) between conformations in each ensemble (Figure 7B, Supporting Information Table S38). Additionally, and as proposed for compounds that behave as molecular chameleons,[13, 15] the SA 3D PSAs was lower for each of the four drugs in chloroform than in water. The differences were large (25-30 Å^2) between the major conformers of roxithromycin, telithromycin and spiramycin, as might be expected from their greater flexibility, but just over 3 Å^2 for the rigid rifampicin.

Inspection of the major conformations of roxithromycin in water and chloroform reveals that the reduction in SA 3D PSA between solvents usually originates from formation of intramolecular hydrogen bonds between the oxime side chain and hydroxy groups of the macrocycle core. For telithromycin SA 3D PSA was reduced in chloroform due to folding of the aromatic side chain over the core of the macrocycle. The reduction for spiramycin originated both from formation of intramolecular hydrogen bonds between the mycaminose moiety and the macrocycle core, and from contacts between hydrophobic parts of the two saccharide moieties, in chloroform.

Deprotonation of roxithromycin, telithromycin and spiramycin, and transformation of rifampicin from its zwitterionic to its non-ionic form, is assumed to occur when the compounds transition from an aqueous environment into a cell membrane, and should be expected to contribute to the reductions in SA 3D PSA. Calculation of the difference in SA 3D PSA between the two charge states for the major conformations of each compound allowed us to estimate this contribution to be approximately 5-10 Å^2 for roxithromycin, telithromycin and spiramycin, and 5 Å^2 for rifampicin (Supporting Information Table S38). Formation of intramolecular interactions thus appears to provide the major part of the reduction in SA 3D PSA for roxithromycin, telithromycin and spiramycin, while deprotonation provides a smaller contribution. For rifampicin, the reduction in SA 3D PSA originates only from the charge redistribution.

Correlations to cell permeability

Cell permeability and aqueous solubility are two of the most important properties that determine to what extent a potential drug is absorbed upon oral administration. The Caco-2 cell model is the most widely used model for oral absorption.[59] It allows determination of passive, transcellular permeabilities when a cocktail of inhibitors of the three major efflux transporters in the intestinal epithelium is employed. In this assay the permeabilities of the four macrocyclic drugs spanned a wide range from high (roxithromycin) via intermediate (telithromycin) to low or very low (rifampicin and spiramycin) (Table 4). In contrast, all four drugs had very high (roxithromycin and telithromycin) or high (spiramycin and rifampicin) aqueous solubilities, most likely due to their charged nature (cf. pKa values, Table 4). In view of the high solubilities, and as it is difficult to develop predictive models for solubility,[60] it was not studied further. We instead focused on the cell permeability of the four drugs.

Table 4. Experimentally determined permeability across Caco-2 cell monolayers, aqueous solubility and pK_a values.

	P_{app} AB+Inh[a] (SEM),[b] ($x10^{-6}$ cm/s)	Solubility[c] (SEM), [b](μM)	pK_a
Roxithromycin[d]	11.9 (1.6)	1510 (24)	9.13
Telithromycin[d]	4.3 (0.1)	1960 (141)	4.91, 8.69
Spiramycin[e]	0.19 (0.029)	327 (46)	>7.26, 8.77
Rifampicin[d]	1.0 (0.1)	183 (8.0)	2.97, 7.50

[a] P_{app} AB+Inh: permeability in the apical-to-basolateral (AB) direction across Caco-2 cell monolayers, determined in the presence of a cocktail of inhibitors of efflux transporters.[15] [b] Standard error based on three to four repeats. [c] Thermodynamic solubility in potassium phosphate buffer, pH 7.4.[15] [d] Data reported previously.[15] [e] Cell permeability and solubility determined in this study as reported previously.[15] Experimentally determined pK_a values were obtained from the literature.[61]

Cell permeability is the results of several sequential processes. Desolvation occurs as the drug leaves the aqueous environment surrounding the cell and interacts with the negatively charged phospholipid head groups before penetrating into the hydrophobic interior of the membrane. It is assumed that neutral species are required to cross the membrane interior, e.g. that amines such as roxithromycin, telithromycin and spiramycin would first undergo deprotonation. This sequence of events is reversed as the drug moves into the cytosol. Various models have been reported for prediction of the relative permeabilities of small sets of macrocyclic peptides and of other compounds in the bRo5 space.[14-15, 62] One is based on the proportionality of permeability to the free energy of transferring the lowest energy state of a cyclic peptide in a low dielectric medium (the low-dielectric conformation, LDC) from water to the membrane interior.[14] Another model focuses on identification of one or several "congruent" conformations, i.e. conformations populated in both water and a membrane-like medium, as the permeating species.[62] In a third model, developed for 18 non-peptidic oral drugs in the bRo5 space, the minimum solvent-accessible 3D polar surface area (SA 3D PSA) was found to correlate well to the cell permeability of the drugs.[15]

We investigated whether the efflux-inhibited (passive) permeabilities of roxithromycin, telithromycin, spiramycin and rifampicin across Caco-2 cell monolayers could be explained by the models outlined above, based on the conformations in their solution ensembles. The low-dielectric conformation for each drug was identified by single-point quantum mechanical energy calculations for the conformations adopted in chloroform (Supporting Information Section 14). Both roxithromycin and rifampicin have congruent conformations, while the conformations most similar by RMSD between chloroform and water were used as congruent for telithromycin and spiramycin (Supporting Information Section 14). After identification of the relevant conformations the free energy of transferring them from water to chloroform ($\Delta G_{transfer}$) was correlated to the passive permeabilities of the four drugs. Excellent correlations were obtained for all compounds both when $\Delta G_{transfer}$ was calculated for the low-dielectric conformations and the congruent conformations (Figure 8). It is noteworthy that these models were obtained with roxithromycin, telithromycin and spiramycin having their tertiary amines protonated, and with rifampicin as a zwitterion. When neutral forms were used, the correlation to permeability was poor using the low-dielectric conformation (r^2 = 0.29) and somewhat lower than for the protonated form when using the congruent conformations (r^2 = 0.84, Supporting Information Figure S16).

We propose that better models were obtained for the charged forms because of the presence of tertiary amines in three of the macrocycles. This functional group was recently highlighted to have a positive impact on the permeability of a collection of drug-like macrocycles,[63] most likely due to attractive interactions with the negatively charged phospholipid head groups of the cell membrane. The protonated tertiary amines could then either be sufficiently lipophilic to cross the hydrophobic interior of the cell membrane, or become deprotonated before crossing it. The SA 3D PSA of both the low-dielectric conformation and the congruent conformations were also found to correlate well to cell permeability (r^2 appr. 0.80, Supporting Information Figure S23), while the correlation to TPSA was poor (r^2 = 0.01, Supporting Information, Figure S24).

Conclusion

Drugs in the bRo5 space have been hypothesized to behave as molecular chameleons based on analysis of crystal structures or computational studies,[11, 13, 15] but experimental support for this has so far been limited to the cyclic peptide cyclosporin A.[11, 16] This study is the first to provide comprehensive experimental and theoretical evidence that non-peptidic bRo5 drugs behave as molecular chameleons. Solution ensembles were determined for four macrocyclic antibacterial agents using a validated NMR technique. Major differences were found between the ensembles determined in aqueous and non-polar solutions for roxithromycin, telithromycin and spiramycin. Ensembles in water, including the most populated conformation for each drug, were significantly more polar as revealed by their solvent accessible 3D PSA than those in chloroform. The conformations in chloroform were more compact, i.e. had smaller radius of gyration (R_{gyr}), than those in water. Rifampicin showed a similar behaviour, but was found to be much more rigid with less pronounced differences between the environments. The adoption of ensembles that differ in polarity between environments is likely to be an important factor in explaining how compounds in bRo5 space can display both high aqueous solubility and cell membrane permeability, as has recently been hypothesized.[13, 15]

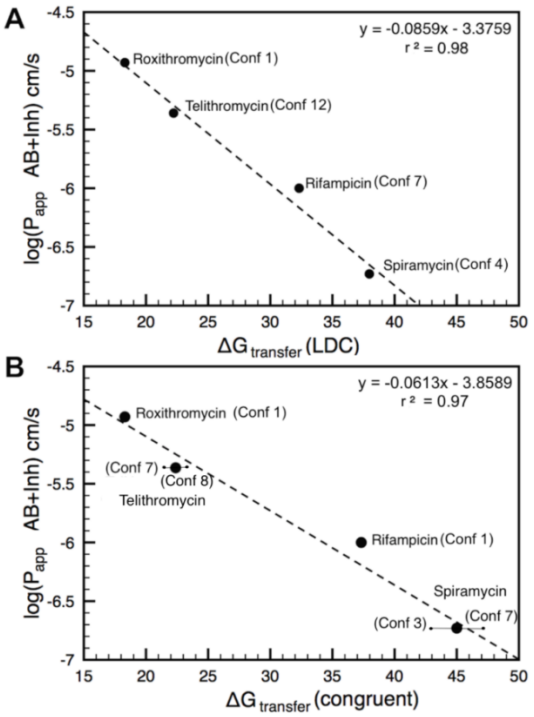

Figure 8 Efflux-inhibited permeability of the four drugs across a Caco-2 epithelial cell monolayer [log (P_{app} AB + Inh) cm/s] and its correlation to (**A**) the free energy of transferring the lowest energy state of each drug in $CDCl_3$ (the low-dielectric conformation, LDC) from water to $CDCl_3$, and (**B**) the free energy of transferring the congruent conformation (the conformation populated in both water and $CDCl_3$) of each drug in $CDCl_3$ from water to $CDCl_3$. The number of the conformation identified as the LDC and of the congruent conformation(s) is given in parentheses after the name of each compound in panels A and B, respectively. For telithromycin and spiramycin the numbers of the two most similar conformations (by RMSD) are given at the whiskers of the error bars in panel B. The conformations to the left belongs to the aqueous ensemble, the ones to the right to chloroform. The average $\Delta G_{transfer}$ for transferring the two conformations from water to chloroform has then been used in the correlation. All compounds had SEM for log (P_{app} AB + Inh) within the size of the symbols.

Our data supports that the target bound structure of a drug can be expected to be populated also in solution.[20, 24, 51-54] Interestingly, telithromycin binds to ribosomes of different organisms in conformations that show striking diversity, several of which are present in solution in a measurable population. The target bound conformations of spiramycin and rifampicin also differ between targets from different organisms, but to a lesser extent. Notably, rifampicin binds to different proteins from different organisms in different conformations. Consequently, an

appropriate conformation flexibility of drugs in the bRo5 space appears important for their ability to bind targets that vary in structure, in addition to providing chameleonicity that balances their solubility and cell permeability. Possibly, this flexibility may also be important for polypharmacology.

The relative, passive permeabilities of the four drugs is in excellent agreement with models developed for cyclic peptides and a set of drugs in the bRo5 space.[14-15, 62] Our results corroborate the suggestion that the conformation having the lowest energy in a low dielectric medium, mimicking the cell membrane, has a key role for cell permeability.[14] Our data also supports the hypothesis that the congruent conformations, i.e. those common to aqueous and apolar environments, could be the permeating species.[62] In addition, it highlights the importance of the surface accessible 3D PSA for cell permeability.[15]

All four drugs adopt only a limited number of conformations in environments that differ in polarity, usually including the target bound state. We therefore conclude that molecular chameleons have a flexibility in between that of highly flexible molecules and those adopting a stable 3D structure. In spite of populating relatively few conformations, the ensembles of all but the comparably rigid rifampicin display major differences in size and polarity between different environments. This is due to synergistic structural adjustments of the macrocycle core and its attached side chains in roxithromycin, telithromycin and spiramycin. Rifampicin differs as it only has a small, fairly rigid side chain, whereas its macrocyclic core is equally or more flexible than those of the other three drugs. Conformations adopted in chloroform are typically stabilized by intramolecular hydrogen bonds and/or van der Waals interactions that reduce their polar surface area as compared to those of the aqueous ensembles. In addition, charge neutralization contributes to the reduction of polar surface area in chloroform.

We propose that the semi-rigidity revealed herein for molecular chameleons is an important element to incorporate in the design of chemical probes and drugs in the bRo5 space directed towards intracellular targets. A recent analysis found that all approved drugs in bRo5 space had between 5 and 20 rotatable bonds.[15] However, further guidelines for flexibility and design of molecular chameleons remain to be established, just as guidelines for other properties required by drugs in bRo5 space. In an optimal chameleon, dynamically formed intramolecular interactions provide major changes in molecular descriptors, such as the solvent accessible 3D polar surface area and the shape, between conformations. Thereby chameleons may simultaneously display high cell permeability and aqueous solubility. Their semi-rigidity may also reduce the entropic cost for entering a cell membrane, while also providing potent target binding. Recently, both intramolecular hydrogen bonds[64-65] and NH-π interactions[66] have been used in the design of orally administered and cell permeable drug candidates. Although such examples are still rare, they constitute the first step towards the wider incorporation of molecular chameleonicity in design of chemical probes and drugs.

Experimental Section

NMR spectroscopy

Roxithromycin and spiramycin were purchased as free amines from Selleckchem. Telithromycin, as a free amine, was obtained from TOKU-E, while rifampicin was from Sigma. All compounds had a purity >95%. The compounds were dissolved in $CDCl_3$ and D_2O, and the pH was adjusted to appr. 7.0 for the D_2O solutions. Proton assignments in D_2O and $CDCl_3$ were derived from TOCSY, NOESY, COSY, HSQC and HMBC spectra recorded at 25 °C on a 900 MHz Bruker Avance III HD NMR spectrometer equipped with a TCI cryogenic probe. All $^3J_{HA\text{-}HN}$ coupling constants were measured from ^{1}H NMR spectra, from which backbone dihedral angles were derived via the Karplus equation.[67] Interproton distances were derived from NOE build-up rates according to the initial rate approximation.[68-69] NOESY spectra were recorded without solvent suppression, with mixing times of 100, 200, 300, 400, 500, 600 and 700 msec. The relaxation delay was set to 2.5 s, and 16 scans were recorded with 8192 points in the direct dimension and 512 points in the indirect dimension. Geminal methylene protons (1.78 Å), or if unavailable, CH_3CH fragments (2.57 Å) were used as distance reference. Comparable distances obtained from various methylene proton pairs within the macrocycles indicated the high quality of the data. NOE peak intensities were calculated using normalization of both cross peaks and diagonal peaks according to ([cross peak1 × cross peak2]/[diagonal peak1 × diagonal peak2])$^{0.5}$ equation. At least 5 mixing times giving a linear (r2 > 0.95, typically > 0.98) initial NOE rate for every distance were used to determine distances according to the equation $r_{ij}=r_{ref}(\sigma_{ref}/\sigma_{ij})^{(1/6)}$, where r_{ij} is the distance between protons i and j in Ångström, r_{ref} is 1.78 Å and σ_{ref} and σ_{ij} are the build-up rates for the reference and the i–j proton pair, respectively. ^{1}H assignments, coupling constants, distances and build-ups are given in the Supporting Information, Sections 1 and 2.

Conformational sampling

Theoretical ensembles for the neutral forms of roxithromycin, telithromycin and spiramycin, and the non-ionic form or rifampicin, were obtained from Monte Carlo Molecular Mechanics (MCMM) and Macrocycle Conformational Sampling (MCS) calculations, using the software Macromodel (v.9.1) as implemented in the Schrödinger package. At least two different force fields were used, and both water and chloroform solvent models (Supporting Information, Table S15). In order to provide ensembles covering the entire available conformational space an energy window of 42 kJ mol^{-1} and 50000 Monte Carlo steps were used. The energy minimization was performed using the Polak-Ribiere conjugate gradient (PRCG) algorithm with maximum iteration steps set to 5000. MCS, hybrid of large-scale low-mode (LLMOD) sampling with simulated annealing, was performed using the OPLS-2005 force field, and the GB/SA (water) implicit solvent model. It was set-up with 5000 simulation cycles, 5000 LLMOD search steps, and the energy window for saving structures set at 10 kcal/mol with an RMSD of 0.75 Å for rifampicin, 1.5 Å for roxithromycin and telithromycin, and 2.0 Å for spiramycin. The ensembles from the conformational searches were combined and elimination of redundant conformations by comparisons of the heavy atom coordinates was performed, giving the final ensembles after addition of all available PDB and CSD crystal structures of the studied compound. The generated MCMM-ensembles fulfilled the expression $1-(1-(1/N))^M$ (N = total number of conformers, M = number of search steps) indicating that the available conformational space was fully covered.[17] Further details about the final input ensembles used for NAMFIS are found in the Supporting Information, Sections 3 and 4.

NAMFIS

Solution ensembles were determined by fitting the experimentally measured distances to those back-calculated for the computationally predicted conformations following previously described protocols.[36] CH_2-signals were treated according to the equation $d=(((d_1^{-6})+(d_2^{-6}))/2)^{-1/6}$, and CH_3-signals according to $d=(((d_1^{-6})+(d_2^{-6})+(d_3^{-6}))/3)^{-1/6}$, where $d_{1\text{-}3}$ are the distances from a certain proton to the different yet magnetically equivalent protons. The results were validated within 10% using standard methods, i.e. by the addition of random noise (max 10%) to the experimental data, by the random removal of individual restraints (10%), and by comparison of the experimentally

observed and back-calculated distances. Macrocycle core conformations were classified as different if their heavy atom root-mean-square deviation (RMSD) was >0.5 Å,[70-71] while a >0.75 Å heavy atom cut off was used for the overall macrocycle including side chains. All conformations for each macrocycle in the two solvents, with the corresponding molar fractions, are given in the Supporting Information, Section 6.

Refinement of conformations

Conformations obtained from the NAMFIS analysis were imported into MOE 2015.10 (Chemical Computing Group, www.chemcomp.com)[72] and were relaxed in the MMFF94x force field with maximum RMSD deviation of ≤ 0.5 Å from its original conformation. Protonation states (neutral and charged forms for roxithromycin, telithromycin and spiramycin; non-ionic and zwitterionic for rifampicin) of each compound in each conformation were manually adjusted according to the compound´s pK_a values (Table 4). For rifampicin, no quantifiable NOE distances were obtained for piperazine side chain. Therefore the geometry of the piperazine side chain in conformations 1 and 6, which are not identical to crystal structures, was calculated by single point energy minimization with DFT B3LYP/6-31G** using the Jaguar tool[73-74] (Supporting Information, Section 10). The final conformations 1 and 6 were subsequently used for RMSD, energy and properties calculations, as for all other conformations.

RMSD calculations

The RMSD metric was calculated to compare the conformations obtained from the NAMFIS analysis, within ensembles, and to X-ray crystal structures. RMSD values were calculated using the OpenEye toolkit[75] (rmsd.py) and Superposition tool (superimposed by SMARTS) in the Maestro module[76] for the heavy atoms of the whole molecule (macrocylic core with side chains) and the macrocylic core, respectively (Supporting Information, Sections 7 and 11).

Molecular property calculations

Radius of gyration (R_{gyr}) was calculated using MOE (v2015.10). Solvent accessible three-dimensional polar surface area (SA 3D PSA) was calculated with PyMol v1.7.4[77] from the solvent accessible surface area defined using a solvent probe radius of 1.4 Å. In addition to polar atoms (O, N, and attached H), absolute partial charges were calculated with the B3LYP/6-31G** method in the Jaguar tool (available in the Schrödinger suite)[73-74] using a partial charges threshold >1.0. Further details on 3D PSA calculation has been reported elsewhere.[15] Calculated values of R_{gyr} and SA 3D PSA are given in the Supporting Information, Sections 12 and 13.

QM calculations

The refined conformations (in the neutral and charged forms for roxithromycin, telithromycin and spiramycin, and in non-ionic and zwitterionic form for rifampicin) were imported into the Maestro module available in the Schrödinger suite and used for SPE (single-point energy) calculations. All conformations from the chloroform ensembles of all four compounds, and conformations 7 and 3 in the aqueous ensembles of telithromycin and spiramycin, respectively, were used for SPE calculations. All QM calculations were performed using the Jaguar tool.[73-74] Energy calculation parameters were from the B3LYP/6-31G** basis set with the PB solvation model[78-79] (ε = 4.8 and probe radius 2.5 Å for chloroform and ε = 80.3 with probe radius 1.4 Å for water). The “accurate” level of Jaguar, which corresponds to tighter convergence thresholds, was used together with the default values of other settings. Calculated SPE values are given in the Supporting Information, Section 14.

Aqueous solubility and cell permeability

The thermodynamic solubility of spiramycin was determined in potassium phosphate buffer, pH 7.4. Passive-diffusive permeability (Papp AB+Inh) across intestinal epithelial cell monolayers was measured in the Caco-2 cell model at pH 7.4 in the apical-to-basolateral (AB) direction in the presence of a cocktail of three inhibitors that target the three major efflux transporters. Both solubility and cell permeability were determined using the procedures reported previously for roxithromycin, telithromycin and rifampicin.[15]

Acknowledgements

The authors would like to acknowledge support from Maria Backlund at Uppsala Drug Optimization and Pharmaceutical Profiling, Department of Pharmacy, Uppsala University. This study made use of the NMR Uppsala infrastructure, which is funded by the Department of Chemistry - BMC and the Disciplinary Domain of Medicine and Pharmacy. We are grateful for access to 800 MHz and 900 MHz NMR instruments at the Swedish NMR Centre. We also thank OpenEye scientific software and ChemAxon for providing academic licenses. This work was funded by grants from the Swedish Research Council (grant no. 2016-05160; J.K. and 2016-03602; M.E.).

Keywords: Antibiotics • Cell permeability • Macrocycles • Molecular chameleon • NMR spectroscopy.

[1] C. A. Lipinski, F. Lombardo, B. W. Dominy and P. J. Feeney, *Adv. Drug Deliv. Rev.* **1997**, *23*, 3-25.
[2] A. L. Hopkins and C. R. Groom, *Nature Rev. Drug Disc.* **2002**, *1*, 727-730.
[3] S. Surade and Tom L. Blundell, *Chem. Biol* **2012**, *19*, 42-50.
[4] B. C. Doak, B. Over, F. Giordanetto and J. Kihlberg, *Chem. Biol* **2014**, *21*, 1115-1142.
[5] E. M. Driggers, S. P. Hale, J. Lee and N. F. Terrett, *Nat. Rev. Drug Discovery* **2008**, *7*, 608-624.
[6] D. A. DeGoey, H.-J. Chen, P. B. Cox and M. D. Wendt, *J. Med. Chem.* **2017**, *61*, 2636-2651.
[7] M. D. Shultz, *J. Med. Chem.* **2019**, *62*, 1701−1714.
[8] E. Valeur, S. M. Gueret, H. Adihou, R. Gopalakrishnan, M. Lemurell, H. Waldmann, T. N. Grossmann and A. T. Plowright, *Angew. Chem. Int. Ed.* **2017**, *56*, 10294-10323.
[9] B. C. Doak, J. Zheng, D. Dobritzsch and J. Kihlberg, *J. Med. Chem.* **2016**, *59*, 2312-2327.
[10] E. A. Villar, D. Beglov, S. Chennamadhavuni, J. A. Porco, D. Kozakov, S. Vajda and A. Whitty, *Nat. Chem. Biol.* **2014**, *10*, 723-732.
[11] A. Alex, D. S. Millan, M. Perez, F. Wakenhut and G. A. Whitlock, *MedChemComm* **2011**, *2*, 669-674.
[12] P. Matsson, B. C. Doak, B. Over and J. Kihlberg, *Adv. Drug Deliv. Rev.* **2016**, *101*, 42-61.
[13] A. Whitty, M. Zhong, L. Viarengo, D. Beglov, D. R. Hall and S. Vajda, *Drug Discov. Today* **2016**, *21*, 712-717.
[14] T. Rezai, J. E. Bock, M. V. Zhou, C. Kalyanaraman, R. S. Lokey and M. P. Jacobsen, *J. Am. Chem. Soc.* **2006**, *128*, 14073-14080.
[15] M. Rossi Sebastiano, B. C. Doak, M. Backlund, V. Poongavanam, B. Over, G. Ermondi, G. Caron, P. Matsson and J. Kihlberg, *J. Med. Chem.* **2018**, *61*, 4189-4202.
[16] C. K. Wang, J. E. Swedberg, P. J. Harvey, Q. Kaas and D. J. Craik, *J. Phys. Chem. B* **2018**, *122*, 2261-2276.
[17] N. Nevins, D. Cicero and J. P. Snyder, *J. Org. Chem.* **1999**, *64*, 3979-3986.
[18] C. Grimmer, T. W. Moore, A. Padwa, A. Prussia, G. Wells, S. Wu, A. Sun and J. P. Snyder, *J. Chem. Inf. Model.* **2014**, *54*, 2214-2223.
[19] E. Danelius, U. Brath and M. Erdélyi, *Synlett* **2013**, *24*, 2407-2410.
[20] E. Danelius, M. Pettersson, M. Bred, J. Min, M. B. Waddell, R. K. Guy, M. Grøtli and M. t. Erdélyi, *Org. Biomol. Chem.* **2016**, *14*, 10386-10393
[21] H. Andersson, H. Demaegdt, G. Vauquelin, G. Lindeberg, A. Karlén, M. Hallberg, M. t. Erdélyi and A. Hallberg, *J. Med. Chem.* **2010**, *53*, 8059-8071.
[22] J. J. Koivisto, E. T. T. Kumpulainen and A. M. P. Koskinen, *Org. Biomol. Chem.* **2010**, *8*, 2103-2116.
[23] P. Thepchatri, D. O. Cicero, E. Monteagudo, A. K. Ghosh, B. Cornett, E. R. Weeks and J. P. Snyder, *J. Am. Chem. Soc.* **2005**, *127*, 12838-12846.
[24] P. Thepchatri, T. Eliseo, D. O. Cicero, D. Myles and J. P. Snyder, *J. Am. Chem. Soc.* **2007**, *129*, 3127-3134.
[25] E. Danelius, R. G. Ohm, Ahsanullah, M. Mulumba, H. Ong, S. Chemtob, M. Erdelyi and W. D. Lubell, *J. Med. Chem.* **2019**, *62*, 11071−11079.
[26] R. Dickman, E. Danelius, S. A. Mitchell, D. F. Hansen, M. Erdelyi and A. T. Tabor, *Chem. Eur. J.* **2019**, *25*, 14572 – 14582.

[27] G. Gramse, A. Dols-Perez, M. A. Edwards, L. Fumagalli and G. Gomila, *Biophys. J.* **2013**, *104*, 1257-1262.
[28] K. Pyta, P. Przybylski, K. Klich and J. Stefańska, *Org. Biomol. Chem.* **2012**, *10*, 8283‑8297.
[29] J. Gharbibenarous, P. Ladam, M. Delaforge and J. P. Girault, *J. Chem. Soc. Perkin Trans. I* **1992**, 1989-2006.
[30] J. Gharbibenarous, M. Delaforge, I. Artaud and J. P. Girault, *Magn. Reson. Chem.* **1990**, *28*, 846-855.
[31] J. Gharbibenarous, M. Delaforge, C. K. Jankowski and J. P. Girault, *J. Med. Chem.* **1991**, *34*, 1117-1125.
[32] J. Gharbibenarous, P. Ladam, M. Delaforge and J. P. Girault, *J. Chem. Soc. Perkin Trans. II* **1993**, 2303-2315.
[33] N. Evrard-Todeschi, J. Gharbi-Benarous, C. Gaillet, L. Verdier, G. Bertho, C. Lang, A. Parent and J. P. Girault, *Bioorg. Med. Chem.* **2000**, *8*, 1579-1597.
[34] P. Alam, J. Barber, R. J. Brennan, K. Kennedy and M. H. H. Tehrani, *Magn. Reson. Chem.* **1995**, *33*, 228-231.
[35] L. Cellai, S. Cerrini, A. Segre, M. Brufani, W. Fedeli and A. Vaciago, *J. Org. Chem.* **1982**, *47*, 2652-2661.
[36] D. O. Cicero, G. Barbato and R. Bazzo, *J. Am. Chem. Soc.* **1995**, *117*, 1027-1033.
[37] V. Poongavanam, E. Danelius, S. Peintner, L. Alcaraz, G. Caron, M. D. Cummings, S. Wlodek, M. Erdelyi, P. C. D. Hawkins, G. Ermondi and J. Kihlberg, *ACS Omega* **2018**, *3*, 11742-11757.
[38] P. C. D. Hawkins, *J. Chem. Inf. Model.* **2017**, 1747−1756.
[39] J. J. Holstein, P. Luger, R. Kalinowski, S. Mebs, C. Paulman and B. Dittrich, *Acta Crystallogr. B* **2010**, *66*, 568-577.
[40] J. A. Dunkle, L. Xiong, A. S. Mankin and J. H. Cate, *Proc. Natl. Acad. Sci. USA* **2010**, *107*, 17152-17157.
[41] D. Bulkley, C. A. Innis, G. Blaha and T. A. Steitz, *Proc. Natl. Acad. Sci. USA* **2010**, *107*, 17158-17163.
[42] Z. Eyal, D. Matzov, M. Krupkin, I. Wekselman, S. Paukner, E. Zimmerman, H. Rozenberg, A. Bashan and A. Yonath, *Proc. Natl. Acad. Sci. USA* **2015**, *112*, E5805-E5814.
[43] D. H. Fong, D. L. Burk, J. Blanchet, A. Y. Yan and A. M. Berghuis, *Structure* **2017**, *25*, 750‑761.
[44] J. L. Hansen, J. A. Ippolito, N. Ban, P. Nissen, P. B. Moore and T. A. Steitz, *Mol. Cell* **2002**, *10*, 117‑128.
[45] A. L. Ibiapino, R. C. Seiceira, A. Pitaluga, A. C. Trindade and F. F. Ferreira, *CrystEngComm* **2014**, *16*, 8555-8562.
[46] M. M. de Villiers, M. R. Caira, J. Li, S. J. Strydom, S. A. Bourne and W. Liebenberg, *Mol. Pharmaceutics* **2011**, *8*, 877-888.
[47] E. A. Campbell, O. Pavlova, N. Zenkin, F. Leon, H. Irschik, R. Jansen, K. Severinov and S. A. Darst, *EMBO J.* **2005**, *24*, 674-682.
[48] X. Qi, W. Lin, M. Ma, C. Wang, Y. He, N. He, J. Gao, H. Zhou, Y. Xiao, Y. Wang and P. Zhang, *Proc. Natl. Acad. Sci. USA* **2016**, *113*, 3803-3808.
[49] D. Garriga, S. Headey, C. Accurso, M. Gunzburg, M. Scanlon and F. Coulibaly, *Proc. Natl. Acad. Sci. USA* **2018**, *115*, 8424-8429.
[50] J. Baysarowich, K. Koteva, D. W. Hughes, L. Ejim, E. Griffiths, K. Zhang, M. Junop and G. D. Wright, *Proc. Natl. Acad. Sci. USA* **2008**, *105*, 4886-4891.
[51] J. Jiménez-Barbero, A. Canales, P. T. Northcote, R. M. Buey, J. M. Andreu and J. F. Díaz, *J. Am. Chem. Soc.* **2006**, *128*, 8757-8765.
[52] D. Altschuh, O. Vix, B. Rees and J. C. Thierry, *Science* **1992**, *256*, 92-94.
[53] R. M. Wenger, J. France, G. Boverman, L. Walliser, A. Widmer and H. Widmer, *FEBS Lett.* **1994**, *340*, 255-259.
[54] M. Erdélyi, B. Pfeiffer, K. Hauenstein, J. Fohrer, J. Gertsch, K.-H. Altmann and T. Carlomagno, *J. Med. Chem.* **2008**, *51*, 1469‑1473.
[55] F. Schluenzen, R. Zarivach, J. Harms, A. Bashan, A. Tocilj, R. Albrecht, A. Yonath and F. Franceschi, *Nature* **2001**, *413*, 814-821.
[56] C. R. W. Guimarães, A. M. Mathiowetz, M. Shalaeva, G. Goetz and S. Liras, *J. Chem. Inf. Model.* **2012**, *52*, 882-890.
[57] P. Narang, K. Bhushan, S. Bose and B. Jayaram, *Phys. Chem. Chem. Phys.* **2005**, *7*, 2364-2375.
[58] D. F. Veber, S. R. Johnson, H.-Y. Cheng, B. R. Smith, K. W. Ward and K. D. Kopple, *J. Med. Chem.* **2002**, *45*, 2615-2623.
[59] P. Artursson, K. Palm and K. Luthman, *Adv. Drug Delivery Rev.* **2001**, *46*, 27-43.
[60] Y. A. Abramov, *Mol. Pharmaceutics* **2015**, *12*, 2126−2141.
[61] S. Sanli, N. Sanli and G. Alsancak, *Acta Chim. Slov.* **2010**, *57*, 980‑987.
[62] J. Witek, S. Wang, B. Schroeder, R. Lingwood, A. Dounas, H.-J. Roth, M. Fouché, M. Blatter, O. Lemke, B. Keller and S. Riniker, *J. Chem. Inf. Model.* **2019**, *59*, 294−308.
[63] B. Over, P. Matsson, C. Tyrchan, P. Artursson, B. C. Doak, M. A. Foley, C. Hilgendorf, S. Johnston, I. Lee, M. D., R. Lewis, P. McCarren, G. Muncipinto, U. Norinder, M. Perry, J. R. Duvall and J. Kihlberg, *Nature Chem. Biol.* **2016**, *12*, 1065-1074.
[64] R. L. Mackman, V. A. Steadman, D. K. Dean, P. Jansa, K. G. Poullennec, T. Appleby, C. Austin, C. A. Blakemore, R. Cai, C. Cannizzaro, G. Chin, J.-Y. C. Chiva, N. A. Dunbar, H. Fliri, A. J. Highton, H. Hui, M. Ji, H. Jin, K. Karki, A. J. Keats, L. Lazarides, Y.-J. Lee, A. Liclican, M. Mish, B. Murray, S. B. Pettit, P. Pyun, M. Sangi, R. Santos, J. Sanvoisin, U. Schmitz, A. Schrier, D. Siegel, D. Sperandio, G. Stepan, Y. Tian, G. M. Watt, H. Yang and B. E. Schultz, *J. Med. Chem.* **2018**, *61*, 9473−9499.
[65] M. G. Yang, Z. Xiao, R. J. Cherney, A. J. Tebben, D. G. Batt, G. D. Brown, J. Chen, M. E. Cvijic, M. Dabros, J. V. Duncia, M. Galella, D. S. Gardner, P. Khandelwal, S. S. Ko, M. F. Malley, R. Mo, J. Pang, A. V. Rose, J. B. Santella III, H. Shi, A. Srivastava, S. C. Traeger, B. Wang, S. Xu, R. Zhao, J. C. Barrish, S. Mandlekar, Q. Zhao and P. H. Carter, *ACS Med. Chem. Lett.* **2019**, *10*, 300−305.
[66] M. Tyagi, V. Poongavanam, M. Lindhagen, A. Pettersen, P. Sjö, S. Schiesser and J. Kihlberg, *Org. Lett.* **2018**, *20*, 5737−5742.
[67] C. A. G. Haasnoot, F. A. A. M. de Leeuw and C. Altona, *Tetrahedron* **1980**, *36*, 2783-2792.
[68] S. Macur, B. T. Farmer and L. R. Brown, *J. Magn. Reson.* **1986**, *70*, 493-499.
[69] H. Hu and K. Krishnamurthy, *J. Magn. Reson.* **2006**, *182*, 173-177.
[70] E. A. Coutsias, K. W. Lexa, M. J. Wester, S. N. Pollock and M. P. Jacobson, *J. Chem. Theory Comput.* **2016**, *12*, 4674-4687.
[71] Q. Wang, S. Sciabola, G. Barreiro, X. Hou, G. Bai, M. J. Shapiro, F. Koehn, A. Villalobos and M. P. Jacobson, *J. Chem. Inf. Model.* **2016**, *56*, 2194-2206.
[72] M. O. E. (MOE) in *Chemical Computing Group ULC, 1010 Sherbooke St. West, Suite #910, Montreal, QC, Canada, H3A 2R7*, *Vol.* **2015**.
[73] A. D. Bochevarov, E. Harder, T. F. Hughes, J. R. Greenwood, D. A. Braden, D. M. Philipp, D. Rinaldo, M. D. Halls, J. Zhang and R. A. Friesner, *Int. J. Quantum Chem.* **2013**, *113*, 2110-2142.
[74] Jaguar in *Vol.* Schrödinger, LLC, New York, NY, **2017.1**.
[75] OpenEyeToolkits in *Vol.* OpenEye Scientific Software, Santa Fe, NM. , **2018**.
[76] Maestro in *Vol.* Schrödinger, LLC, New York, NY, **2017.1**.
[77] PyMOL in *Vol.* The PyMOL Molecular Graphics System, Version 2.0 Schrödinger, LLC., **2017.1**.
[78] C. M. Cortis, J. M. Langlois, M. D. Beachy and R. A. Friesner, *J. Chem. Phys.* **1996**, *105*, 5472-5484.
[79] C. M. Cortis and R. A. Friesner, *J. Comput. Chem.* **1997**, *18*, 1570-1590.

10.1002/chem.201905599

Entry for the Table of Contents

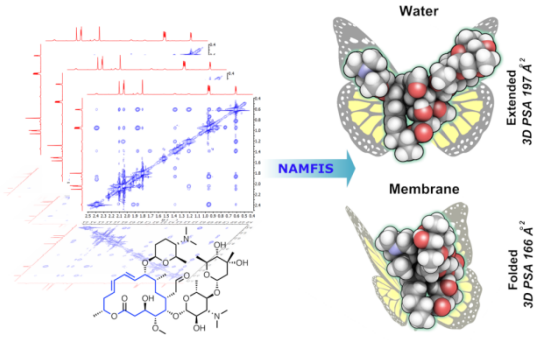

NMR spectroscopy and computational studies reveal that macrocyclic drugs in the beyond rule of 5 chemical space behave as molecular chameleons. This allows them to adapt to the environment and combine otherwise conflicting properties including aqueous solubility, cell permeability and target binding.